

# Polar Linear Canonical Transform in Quaternion Domain

Bo Hu, Yu Zhou, Lei-Da Li, Jian-Ying Zhang\*

School of Information and Electrical Engineering  
China University of Mining and Technology  
Xuzhou, 221116, China

\*Corresponding author: zjycumt@126.com

Jeng-Shyang Pan<sup>1,2</sup>

<sup>1</sup>College of Information Science and Engineering  
Fujian University of Technology  
Fuzhou, 350118, China

<sup>2</sup>Department of Computer Science and Technology  
Harbin Institute of Technology Shenzhen Graduate School  
Shenzhen, 518055, China

Received July, 2015; revised September, 2015

---

**ABSTRACT.** Nowadays, almost all images acquired are in color format. Traditional methods process color images by either transforming them into gray scale or dividing them into red, green, and blue components for independent processing, which is definitely not effective in representing color information. Recently, a novel Polar Linear Canonical Transform (PLCT) with parameters in  $SL(2, \mathbb{R})$  has been reported, which is a generalization of the well-known Polar Harmonic Transform (PHT). However, PLCT is defined on gray-scale images, so it cannot handle color images directly. To solve the problem, this paper generalizes PLCT from complex domain to hypercomplex domain using quaternion algebras, producing the Quaternion Polar Linear Canonical Transform (QPLCT). The performance of QPLCT is then evaluated with Quaternion Fractional Polar Exponential Transform (QPFrET) as an example. The experimental results show that the QPLCT performs better than the commonly used Quaternion form Zernike Moment (QZM) and pseudo-Zernike Moment (QPZM) in terms of image representation capability and numerical stability.

**Keywords:** Orthogonal transforms, Quaternion polar linear canonical transform, Quaternion fractional polar exponential transform, Rotation invariance

---

1. **Introduction.** Nowadays, almost all images acquired are chromatic. However, most of the current image processing algorithms process color images by first converting them into gray scale. An alternative way is to divide color images into red, green and blue channels for independent processing. This definitely loses significant color information and cannot capture the correlation among color channels. In order to solve these problems, quaternion theory has been introduced into color image processing, such as image watermarking [1], sparse representation [2], image quality assessment [3] and image authentication [4]. The use of quaternion-based moment functions to color images has also been proposed recently [5, 6, 7, 8].

Orthogonal moments/transforms have been widely used in image analysis, such as data hiding [9], visual quality assessment [10] and image forensics [11]. Yap *et al.* [12]

introduced the Polar Harmonic Transforms (PHTs) based on trigonometric functions, which are extremely simple to compute. Compared with other orthogonal moments, PHTs have better image representation capability, lower noise sensitivity, and low computational complexity. Since their first appearance, PHTs have been widely used in a variety of applications, such as image watermarking [13] and fingerprint classification [14]. Recently, Qi *et al.* [15] introduced a novel orthogonal transform namely Polar Linear Canonical Transform (PLCT), which is based on the linear canonical transform. It is worthy noting that the Fractional Polar Exponential Transform (PFrET) [16] is a special case of the PLCT. Furthermore, the Polar Complex Exponential Transform (PCET) [12], which is one form of PHT, is a special case of the PFrET.

The advantage of using the quaternion theory is that a color image can be treated as a vector field and processed directly, without losing color information. As a generalization of PCET, PLCT holds all good properties of PHTs. However, the PLCTs can not handle color image in a holistic manner, which restricts its practical applications for color images. In this paper, we generalize PLCTs from the complex domain to the hypercomplex domain using quaternion algebras. We test the performance of the proposed QPLCT on color images and compare its performances with the well-known quaternion form Zernike moments (QZM) and pseudo-Zernike moments (QPZM). Experimental results demonstrate the advantages of the proposed method in terms of image representation capability and numerical stability.

**2. Preliminaries.** In this section, we briefly review the Polar Linear Canonical Transform (PLCT) for gray images and introduce some basic definitions of the quaternion.

**2.1. Definition of PLCT.** Polar Linear Canonical Transform (PLCT) [15] of order  $n$  with repetition  $l$ ,  $|n| = |l| = 0, 1, 2, \dots, \infty$ , is defined as

$$\begin{aligned} M_{nl}^A &= \frac{1}{\pi} \int_0^{2\pi} \int_0^1 \overline{H_{nl}^A(r, \theta)} f(r, \theta) r dr d\theta \\ &= \frac{1}{\pi} \int_0^{2\pi} \int_0^1 \overline{R_n^A(r) e^{il\theta}} f(r, \theta) r dr d\theta, \end{aligned} \quad (1)$$

where  $H_{nl}^A(r, \theta)$  denotes the kernel consisting of an angular part  $e^{il\theta}$  and a radial part  $R_n^A(r)$  with  $A = \begin{bmatrix} a & b \\ c & d \end{bmatrix} \in SL(2, \mathfrak{R})$ ;  $R_n^A(r) = \exp\{-iK_n^A(r)\} = \exp\{\frac{-i}{2b}[d(2\pi nb)^2 - 4\pi nbr^2 + ar^4]\}$ , and  $\bar{\cdot}$  denotes the complex conjugate.

It is obvious that the component  $b$  of  $A$  is not equal to zero, otherwise the transform is not rational. Moreover,  $|H_{n,l}^A(r, \theta)| \neq |H_{-n,-l}^A(r, \theta)|$  and  $|M_{n,l}^A(r, \theta)| \neq |M_{-n,-l}^A(r, \theta)|$  if  $A \neq \begin{bmatrix} 0 & b \\ -1/b & 0 \end{bmatrix}$ .

The radial part satisfies the orthogonality condition:

$$\int_0^1 R_n^A(r) \overline{R_{n'}^A(r)} r dr = \frac{1}{2} \delta_{nn'}, \quad (2)$$

and the whole kernels satisfy

$$\int_0^{2\pi} \int_0^1 H_{nl}^A(r, \theta) \overline{H_{n'l'}^A(r, \theta)} r dr d\theta = \pi \delta_{nn'} \delta_{ll'}. \quad (3)$$

Since the kernels  $H_{nl}^A(r, \theta)$  satisfy the orthogonality condition, so the PLCT is an orthogonal transform. In addition, the series  $\{\exp(ik\pi t/T), |k| = 0, 1, 2, \dots, \infty\}$  is a set of

completely orthogonal basis on  $t \in [0, 2T]$ . Hence, the kernels  $H_{nl}^A(r, \theta)$  of PLCT are complete in  $[0, 1] \times [0, 2\pi]$ .

When  $A = \begin{bmatrix} \cos \alpha & \sin \alpha \\ -\sin \alpha & \cos \alpha \end{bmatrix}$ , PLCT becomes the PFrET:

$$M_{nl}^\alpha = \frac{1}{\pi} \int_0^{2\pi} \int_0^1 \overline{H_{nl}^\alpha(r, \theta)} f(r, \theta) r dr d\theta, \tag{4}$$

with the kernel

$$\begin{aligned} H_{nl}^\alpha(r, \theta) &= R_n^\alpha(r) e^{i\ell\theta} \\ &= \exp\left\{-\frac{i}{2}[(2\pi n \sin \alpha)^2 + r^4] \cot \alpha + i2\pi n r^2\right\} e^{i\ell\theta}, \end{aligned} \tag{5}$$

where  $\alpha \in [0, 2\pi]$ , except for  $0, \pi, 2\pi$ . Moreover, when  $R_n^{\frac{\pi}{2}}(r) = \exp\{i2\pi n r^2\}$  with  $\alpha = \pi/2$ , PFrET becomes the PCET [12].

The PLCT is defined continuously in a unit circle domain. For an  $M \times N$  image  $g(p, q)$ , it is first transformed into the unit domain  $(x_p, y_q) \in [-1, 1] \times [-1, 1]$ :

$$x_p = \frac{p - M/2}{M/2}, y_q = \frac{q - N/2}{N/2}. \tag{6}$$

Then the PLCTs can be computed as

$$\begin{aligned} M_{nl}^A &= \frac{1}{\pi} \sum_{p=0}^{M-1} \sum_{q=0}^{N-1} \overline{H'_{nl}(x_p, y_q)} f'(x_p, y_q) \Delta x \Delta y \\ &= \frac{4}{\pi MN} \sum_{p=0}^{M-1} \sum_{q=0}^{N-1} \overline{H'_{nl}(x_p, y_q)} f'(x_p, y_q), \end{aligned} \tag{7}$$

where  $f'(x_p, y_q) = g[p, q]$ ,  $x_p^2 + y_q^2 \leq 1$ , and  $\Delta x = 2/M, \Delta y = 2/N$ .

**2.2. Quaternion Algebra.** Quaternions, a generalization of the complex numbers, were introduced by the mathematician Hamilton in 1843 [17]. A quaternion with one real part and three imaginary parts can be written as follows:

$$q = a + bi + cj + dk, \tag{8}$$

where  $a, b, c$  and  $d$  are real numbers, and  $i, j, k$  are three imaginary units obeying the following rules:

$$i^2 = j^2 = k^2 = -1, \tag{9}$$

$$ij = -ji = k, jk = -kj = i, ki = -ik = j. \tag{10}$$

As shown in Eq.(10), the quaternion multiplication is not commutative. If  $a = 0$ , then  $q = bi + cj + dk$  is called a pure quaternion, and if  $q$  has a unit norm ( $|q| = 1$ ), then  $q$  is called unit pure quaternion.

The conjugate and modulus of a quaternion are respectively defined by

$$\bar{q} = a - bi - cj - dk. \tag{11}$$

$$|q| = \sqrt{a^2 + b^2 + c^2 + d^2}. \tag{12}$$

For any two quaternions  $p$  and  $q$ ,  $\overline{pq} = \bar{q} \cdot \bar{p}$  holds. Euler's formula holds for quaternions, namely  $e^{q\varphi} = \cos \varphi + q \sin \varphi$ , with  $|e^{q\varphi}| = 1$ . In [18], Sangwine proposed to encode the

three channel components of a RGB image using the three imaginary parts of a pure quaternion. In other words, a RGB format color image can be represented as

$$f(x, y) = f_R(x, y)i + f_G(x, y)j + f_B(x, y)k, \tag{13}$$

where  $f_R(x, y)$ ,  $f_G(x, y)$ , and  $f_B(x, y)$  represent the red, green and blue components, respectively. A more complete discussion about the properties of quaternion can be found in [19].

### 3. Quaternion Polar Linear Canonical Transform.

**3.1. Definition of QPLCT.** Let  $f(r, \theta)$  be a RGB image defined in polar coordinates, we define the left-side Quaternion Polar Linear Canonical Transform (QPLCT) of order  $n$  with repetition  $l$  as

$$\begin{aligned} M_{nl}^L &= \frac{1}{\pi} \int_0^{2\pi} \int_0^1 \exp\{\mu K_n^A(r)\} e^{-\mu l \theta} f(r, \theta) r dr d\theta \\ &= \frac{1}{\pi} \int_0^{2\pi} \int_0^1 e^{\frac{\mu}{2b} [d(2\pi nb)^2 - 4\pi n b r^2 + a r^4]} e^{-\mu l \theta} f(r, \theta) r dr d\theta, \end{aligned} \tag{14}$$

where  $\mu$  is a unit pure quaternion, which is  $\mu = (i + j + k)/\sqrt{3}$  in this paper.

The right-side QPLCT can be obtained by reversing the orders of image and transform kernel in Eq.(14):

$$M_{nl}^R = \frac{1}{\pi} \int_0^{2\pi} \int_0^1 f(r, \theta) \exp\{\mu K_n^A(r)\} e^{-\mu l \theta} r dr d\theta. \tag{15}$$

A color image can be reconstructed by its QPLCT coefficients, and the reconstructions based on left-side and right-side QPLCT coefficients can be written as follows:

$$f(r, \theta) = \sum_{n=-\infty}^{+\infty} \sum_{l=-\infty}^{+\infty} \exp\{-\mu K_n^A(r)\} e^{\mu l \theta} M_{nl}^L, \tag{16}$$

$$f(r, \theta) = \sum_{n=-\infty}^{+\infty} \sum_{l=-\infty}^{+\infty} M_{nl}^R \exp\{-\mu K_n^A(r)\} e^{\mu l \theta}. \tag{17}$$

**3.2. Relationship Between Left-Side and Right-Side QPLCTs.** In Eq.(14), if  $A = \begin{bmatrix} 0 & b \\ -1/b & 0 \end{bmatrix}$ , it becomes QPCET. In [20], Li has analyzed the relationship between the left-side and right-side QPCET, namely  $\overline{M_{n,l}^L} = -M_{-n,-l}^R$ . On the contrary, if  $A \neq \begin{bmatrix} 0 & b \\ -1/b & 0 \end{bmatrix}$ , we have

$$\begin{aligned} \overline{M_{n,l}^L} &= \frac{1}{\pi} \int_0^{2\pi} \int_0^1 \overline{f(r, \theta) \exp\{-\mu K_n^A(r)\} e^{\mu l \theta}} r dr d\theta \\ &= -\frac{1}{\pi} \int_0^{2\pi} \int_0^1 f(r, \theta) \exp\{-\mu K_n^A(r)\} e^{\mu l \theta} r dr d\theta, \end{aligned} \tag{18}$$

$$\begin{aligned} \overline{M_{n,l}^R} &= \frac{1}{\pi} \int_0^{2\pi} \int_0^1 \exp\{-\mu K_n^A(r)\} e^{\mu l \theta} \overline{f(r, \theta)} r dr d\theta \\ &= -\frac{1}{\pi} \int_0^{2\pi} \int_0^1 \exp\{-\mu K_n^A(r)\} e^{\mu l \theta} f(r, \theta) r dr d\theta. \end{aligned} \tag{19}$$

Based on Eq.(18) and Eq.(19), we know that the left-side and right-side QPLCTs are related by  $M_{n,l}^L(\mu) = -\overline{M_{n,l}^R(-\mu)}$  and  $M_{n,l}^R(\mu) = -\overline{M_{n,l}^L(-\mu)}$ .

**3.3. Rotation Invariants.** Let  $f'$  be the rotated version of  $f$ , i.e,  $f'(r, \theta) = f(r, \theta - \alpha)$ , where  $\alpha$  denotes the rotation angle, then the QPLCTs of the two images are related by

$$\begin{aligned}
 M_{nl}^L(f') &= \frac{1}{\pi} \int_0^{2\pi} \int_0^1 e^{-\mu l \theta} \exp\{\mu K_n^A(r)\} f'(r, \theta) r dr d\theta \\
 &= \frac{1}{\pi} \int_0^{2\pi} \int_0^1 e^{-\mu l \theta} \exp\{\mu K_n^A(r)\} f(r, \theta - \alpha) r dr d\theta \\
 &= \frac{1}{\pi} \int_0^{2\pi} \int_0^1 e^{-\mu l(\theta + \alpha)} \exp\{\mu K_n^A(r)\} f(r, \theta) r dr d\theta \\
 &= e^{-\mu l \alpha} \frac{1}{\pi} \int_0^{2\pi} \int_0^1 e^{-\mu l \theta} \exp\{\mu K_n^A(r)\} f(r, \theta) r dr d\theta \\
 &= e^{-\mu l \alpha} M_{nl}^L(f).
 \end{aligned} \tag{20}$$

Likewise, the right-side QPLCTs are related by  $M_{nl}^R(f') = M_{nl}^R(f) e^{\mu l \alpha}$ . Therefore, the modulus of QPLCT coefficient is invariant to image rotation.

When computing the rotation invariants, modulus only contain part of the moment information, because the phase information is not considered. In this paper, we define a new rotation invariant.

**Theorem 3.1.** *The scalar  $\Phi_{nm}^l(f) = \overline{M_{nl}^L(f)} M_{ml}^L(f)$  is invariant to image rotation for any order  $n$  and  $m$  with repetition  $l$ , which satisfy  $|n| + |l| \leq T$  and  $|m| + |l| \leq T$ .*

**Proof:** Let  $f'$  be any rotated version of  $f$ , we have:

$$\begin{aligned}
 \Phi_{nm}^l(f') &= \overline{M_{nl}^L(f')} M_{ml}^L(f') \\
 &= \overline{M_{nl}^L(f)} e^{\mu l \alpha} e^{-\mu l \alpha} M_{ml}^L(f) \\
 &= \overline{M_{nl}^L(f)} M_{ml}^L(f) \\
 &= \Phi_{nm}^l(f).
 \end{aligned} \tag{21}$$

Similarly, we have  $\Phi_{nm}^l(f) = M_{nl}^R(f) \overline{M_{ml}^R(f)}$ . In fact, if  $n = m$ ,  $\Phi_{nl}^L(f) = \overline{M_{nl}^L(f)} M_{nl}^L(f) = |M_{nl}^L(f)|^2$ . For right-side QPLCTs,  $\Phi_{nl}^R(f) = M_{nl}^R(f) \overline{M_{nl}^R(f)} = |M_{nl}^R(f)|^2$ .

**4. Experiments.** In this section, several experiments are carried out to test the performance of the proposed QPLCT, with QPFrET as an example. We will first discuss the impact of the parameter  $\alpha$ . Then image reconstruction using QZM, QPZM and QPFrET are carried out to test their image representation capabilities. Finally, we validate the rotation invariance of QPFrET. Thirty test images from CSIQ [21] database with size  $128 \times 128$  are used to conduct the experiments, which are shown in Fig.1. In the image reconstruction experiment, the difference between an image and its reconstructed version is measured using the Root-Mean-Squared Error (RMSE), which is defined as follows:

$$\text{RMSE} = \sqrt{\frac{\sum_{x'^2+y'^2 \leq 1} [f(x, y) - \widehat{f}(x, y)]^2}{|\{(x', y') | x'^2 + y'^2 \leq 1\}|}}. \tag{22}$$

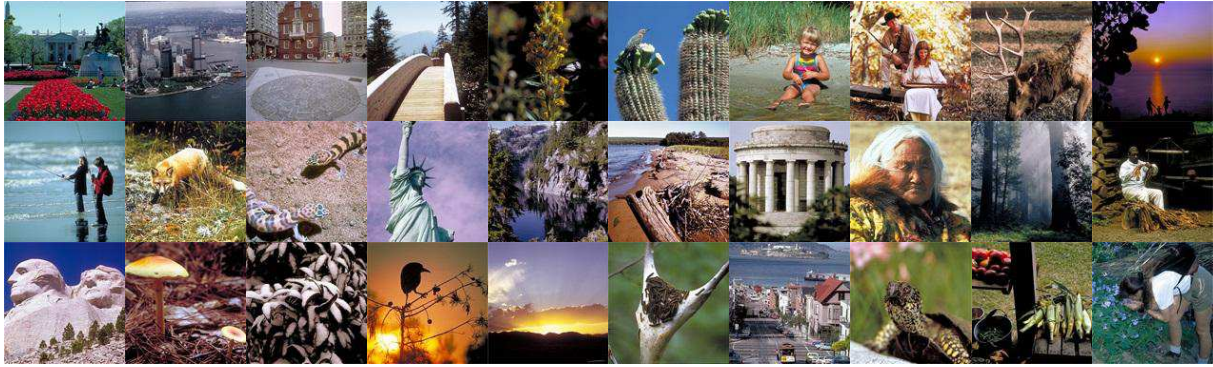


FIGURE 1. Thirty test images used in the experiments.

**4.1. Impact of Parameter  $\alpha$ .** In this subsection, we show the impact of parameter  $\alpha$  on the image reconstruction ability of QPFrETs. Considering  $\cot(\alpha) = \cot(\alpha + \pi)$  and  $\sin(\alpha) = -\sin(\alpha + \pi)$  when  $\alpha \in (0, \pi)$ , then we have  $H_{nl}^\alpha(r, \theta) = H_{nl}^{\alpha+\pi}(r, \theta)$ . So, we only discuss  $\alpha \in (0, \pi)$ . In this experiment, we use different  $\alpha$  values to compute the QPFrETs and approximate images are reconstructed. Then the RMSE values are calculated to measure the distortions, which can be used to evaluate the image representation abilities. The simulation results are listed in Table 1.

TABLE 1. Impact of Parameter  $\alpha$ 

$\alpha \backslash NM$	41	145	313	545	1013	1405	1861
$0.2\pi$	39.3719	32.5377	28.5646	25.6383	22.3567	20.7317	19.3072
$0.5\pi$	39.4010	32.5609	28.5875	25.6654	22.3932	20.7709	19.3479
$0.7\pi$	39.3750	32.5426	28.5722	25.6504	22.3759	20.7540	19.3310

Table 1 shows that different parameters  $\alpha$  with the same *Number of Moments* ( $NM$ ) have limited influence on the RMSE values. It is also observed that the QPFrETs have good image representation capability and show fine numerical stability, regardless of choice of parameters  $\alpha$ .

**4.2. Image Representation.** Image reconstruction is carried out in this subsection. In this experiment, QZM, QPZM and QPFrET coefficients of the lenna image are first calculated. Then the image is reconstructed according to Eq.(16). Let  $T$  be a constant, we have limited the number of moments used in reconstruction based on the following: QZMs:  $n - |l| = \text{even}, |l| \leq n \leq T$ ; QPZMs:  $|l| \leq n \leq T$ ; QPFrETs:  $|l| + |n| \leq T$ .

The reconstruction results are shown in Fig.2. As more moments are added to the reconstruction process, the reconstructed images get closer to the original image. In order to verify the image representation capability of the QPFrETs, 30 test images were used. In Fig.3, we show plots of the average RMSE values of the 30 images. For QZM, the numerical stability breaks down when the number of moments is increased to 460. Similar phenomenon happens to QPZM, which does not happen to QPFrET. It can be observed that the QPFrETs have better numerical stability than QZMs and QPZMs.

**4.3. Rotation Invariance.** In order to verify the rotation invariance of QPFrET, the Lenna image is resized to  $128 \times 128$ , based on which seven rotated versions are produced, which are shown in Fig.4. Then the rotation invariants are calculated, which are listed in Table 2. Note that we set  $\alpha = 0.2\pi$  in this experiment.

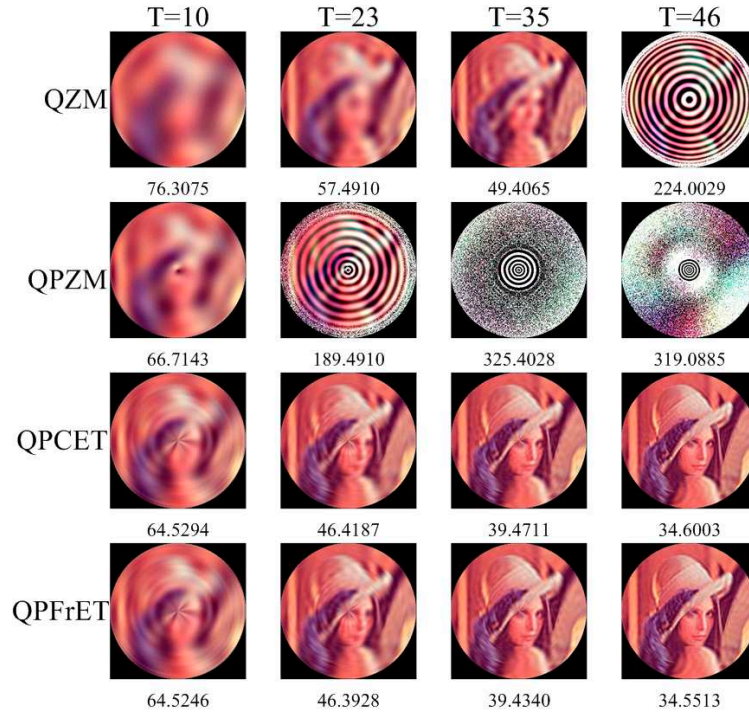


FIGURE 2. Reconstructed images using different types of quaternion moments.

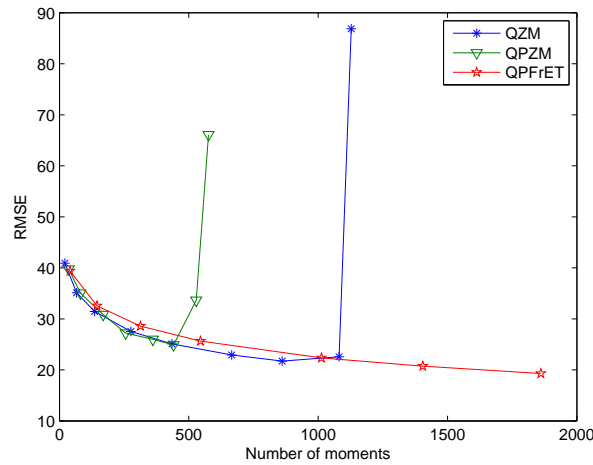


FIGURE 3. Average RMSE values of QZM, QPZM and QPFrET



FIGURE 4. The original image and seven rotated versions of it. From left to right rotation angles are: 0, 30, 60, 120, 150, 210, 280, 330.

TABLE 2. Rotation Invariants of QPFrET

	$ \Phi_{0,-1}^L(f) $	$ \Phi_{0,1}^L(f) $	$ \Phi_{0,3}^L(f) $	$ \Phi_{1,-2}^L(f) $	$ \Phi_{1,-1}^L(f) $	$ \Phi_{1,2}^L(f) $
$0^\circ$	236.4617	368.2300	89.3691	63.6107	71.7578	172.6477
$30^\circ$	233.2333	363.0605	89.0608	62.2914	72.5711	174.4658
$60^\circ$	234.7689	364.1322	88.9331	61.9919	72.1775	171.8471
$120^\circ$	232.5249	362.4330	89.2649	61.9786	72.0885	173.9093
$150^\circ$	234.0379	362.7529	89.0772	62.3589	72.5747	172.0100
$210^\circ$	232.4369	362.1215	88.6749	62.1152	72.5215	174.2891
$280^\circ$	234.9381	364.9644	88.8713	62.6471	73.0832	171.5820
$330^\circ$	234.3537	363.1164	89.0881	62.1695	72.3730	172.0788
$\nu$	234.0944	363.8514	89.0424	62.3954	72.3934	172.8537
$\sigma$	1.3519	1.9952	0.2191	0.5370	0.3965	1.1807
$\sigma/\nu\%$	0.5775	0.5484	0.2461	0.8606	0.5477	0.6831

Table 2 shows the rotation invariants  $\Phi_{nl}^L(f)$  values and the corresponding  $\sigma/\nu\%$ , which indicates the percentage of spread of the  $\Phi_{nl}^L(f)$  values from their corresponding means, where  $\nu$  is their respective sample mean and  $\sigma$  is the sample standard deviation. It can be seen from the table that excellent results have been obtained.

**5. Conclusions.** In this paper, we have proposed the Quaternion Polar Linear Canonical Transform (QPLCT) for color image analysis. The mathematical definitions of QPLCTs are first presented. Then the properties of QPLCTs are discussed with QPFrET as an example. A new form of rotation invariance has also been defined with approved. Finally, the image representation capabilities and numerical stabilities are discussed by experiments on real color images. Experimental results have demonstrated that the proposed QPLCTs have achieved very promising results, and it outperforms the commonly used QZMs and QPZMs in terms of both image representation ability and numerical stabilities. As future works, we will apply the proposed QPLCTs in a variety of applications, such as color image retrieval and color image watermarking.

**Acknowledgment.** This work is supported by the National Natural Science Foundation of China (61379143), the Fundamental Research Funds for the Central Universities (2015QNA66), the S&T Program of Xuzhou City (XM13B119), a project funded by the Priority Academic Program Development of Jiangsu Higher Education Institutions (PAPD), and Jiangsu Collaborative Innovation Center on Atmospheric Environment and Equipment Technology (CICAEET).

## REFERENCES

- [1] T. K. Tsui, X. P. Zhang, and D. Androustos, Color image watermarking using multidimensional Fourier transforms, *IEEE Trans. Information Forensics and Security*, vol. 3, no.1, pp.16–28, 2008.
- [2] Y. Xu, L. C. Yu, H. T. Xu, H. Zhang, and T. Nguyen, Vector Sparse Representation of Color Image Using Quaternion Matrix Analysis, *IEEE Trans. Image Processing*, vol. 24, no.4, pp.1315–1329, 2015.
- [3] A. Kolaman and O. Y. Pecht, Quaternion Structural Similarity: A New Quality Index for Color Images, *IEEE Trans. Image Processing*, vol. 21, no.4, pp.1526–1536, 2012.

- [4] J. Ouyang, G. Coatrieux, and H. Z. Shu, Robust hashing for image authentication using quaternion discrete Fourier transform and log-polar transform, *Digital Signal Processing*, vol. 41, pp.98–109, 2015.
- [5] B. J. Chen, H. Z. Shu, H. Zhang, G. Chen, C. Toumoulin, J. L. Dillenseger, and L. M. Luo, Quaternion Zernike moments and their invariants for color image analysis and object recognition, *Signal Process*, vol. 92, no. 2, pp.308-318, 2012.
- [6] L. Guo and M. Zhu, Quaternion Fourier-Mellin moments for color images, *Pattern Recognition*, vol. 44, no. 2, pp.187-195, 2011.
- [7] Z. H. Shao, H. Z. Shu, J. S. Wu, B. J. Chen, and J. L. Coatrieux, Quaternion Bessel-fourier moments and their invariant descriptors for object reconstruction and recognition, *Pattern Recognition*, vol. 47, no. 2, pp.603-611, 2014.
- [8] B. J. Chen, H. Z. Shu, G. Coatrieux, G. Chen, X. M. Sun, and J. L. Coatrieux, Color Image Analysis by Quaternion-Type Moments, *Journal of Mathematical Imaging and Vision* , vol. 51, no. 1, pp.124-144, 2014.
- [9] J. F. Lu, M. Wang, J. P. Dai, Q. R. Huang, L. Li and C. C. Chang, Multiple watermark scheme based on DWT-DCT quantization for medical images, *Journal of Information Hiding and Multimedia Signal Processing*, vol. 6, no. 3, pp. 458-472, 2015.
- [10] W. Zhang, L. D. Li, H. C. Zhu, D. Q. Cheng, S. C. Chu and J. F. Roddick, No-reference quality metric of blocking artifacts based on orthogonal moments, *Journal of Information Hiding and Multimedia Signal Processing*, vol. 5, no. 4, pp. 701-708, 2014.
- [11] S. A. Thajeel and G. Sulong, A novel approach for detection of copy move forgery using completed robust local binary pattern, *Journal of Information Hiding and Multimedia Signal Processing*, vol. 6, no. 2, pp. 351-364, 2015.
- [12] P. T. Yap, X. D. Jiang, and A. C. Kot, Two-dimensional polar harmonic transforms for invariant image representation, *IEEE Trans. Pattern Anal. Mach. Intell*, vol. 32, no.7, pp.1259–1270, 2010.
- [13] L. D. Li, S. S. Li, A. Abraham, and J. S. Pan, Geometrically invariant image watermarking using Polar Harmonic Transforms, *Information Sciences* , vol. 199, pp: 1-19, Sept. 2012
- [14] M. Liu, X. D. Jiang, A. C. Kot, and P. T. Yap, Application of polar harmonic transforms to fingerprint classification, *Emerging topics in computer vision and its applications*, 2011.
- [15] M. Qi, B. Z. Li, and H. Sun, Image watermarking using polar harmonic transform with parameters in  $SL(2, \mathbb{R})$ , *Signal Processing: Image Communication*, vol.31, pp.161-173, 2015.
- [16] M. Qi, B. Z. Li, and H. Sun, Image watermarking via fractional polar harmonic transforms, *J. Electronic Imaging*, vol.24, no.1, 013004, 2014.
- [17] W. R. Hamilton, Elements of Quaternions , *Longmans Green*, London, U.K, 1866.
- [18] S. J. Sangwine, Fourier transforms of color images using quaternion or hypercomplex numbers, *Electronics Letters*, vol.32, no.21, pp.1979-1980, 1996.
- [19] I. L. Kantor, and A. S. Solodovnikov , Hypercomplex Number: An Elementary Introduction to Algebras, *Springer-Verlag*, New York, 1989.
- [20] Y. N. Li, Quaternion Polar Harmonic Transforms for Color Images, *IEEE Signal Processing Letters*, vol. 20, no. 8, pp.803-806, 2013.
- [21] E. C. Larson, and D. M. Chandler, Most apparent distortion: Full reference image quality assessment and the role of strategy, *J. Electronic Imaging*, vol. 19, no. 1, pp.011006:1-21, 2010.